NASA Technical Memorandum 105975
AIAA–93–0170

Numerical Modeling of Anti-Icing Systems and Comparison to Test Results on a NACA 0012 Airfoil

Kamel M. Al-Khalil and Mark G. Potapczuk
Lewis Research Center
Cleveland, Ohio

Prepared for the
31st Aerospace Sciences Meeting and Exhibit
sponsored by the American Institute of Aeronautics and Astronautics
Reno, Nevada, January 11–14, 1993

Numerical Modeling of Anti-icing Systems and Comparison to Test Results on a NACA 0012 Airfoil

Kamel M. Al-Khalil* and Mark G. Potapczuk†
NASA Lewis Research Center
Cleveland, Ohio 44135

A series of experimental tests were conducted in the NASA Lewis IRT on an electro-thermally heated NACA 0012 airfoil. Quantitative comparisons between the experimental results and those predicted by a computer simulation code were made to assess the validity of a recently developed anti-icing model. An infrared camera was utilized to scan the instantaneous temperature contours of the skin surface. Despite some experimental difficulties, good agreement between the numerical predictions and the experimental results were generally obtained for the surface temperature and the possibility for the runback to freeze. Some recommendations were given for an efficient operation of a thermal anti-icing system.

Nomenclature

C_p = pressure coefficient

C_f = friction coefficient

F = ratio of wetted area to the total surface at a particular streamwise location

FF = freezing fraction: ratio of liquid water that freezes to the total liquid entering a control volume

LWC = liquid Water Content (g/m^3)

MVD = mean volume droplet diameter (μm)

m^o = runback water mass flow rate

P = static pressure

q'' = rate of heat transfer per unit area at the of the skin surface

s = surface distance from stagnation (positive on the upper surface and negative on the lower)

T = temperature

V = Velocity

x/c = ratio of chordwise distance to the airfoil chord

β = droplet collection efficiency

λ = ratio of rivulet width to wetness factor, or distance between two surface streamlines

θ = rivulet contact angle with the solid surface

ρ = density

τ = aerodynamic shear force at the skin surface

Subscripts

surf = outer surface of the aircraft skin

∞ = free stream

I. Introduction

Aircraft icing problems have been encountered for several decades during flights in adverse weather conditions. Aerodynamic penalties as well as the dramatic accidents associated with ice accreted on critical aircraft surfaces have led many researchers to study this phenomenon. Extensive studies are required in order to better understand the icing process and to accurately develop analytical models and computational codes for use as analysis and design tools. The cost involved to develop these codes is far less than the cost of obtaining a complete experimental database.

De-icing systems have been mainly developed to protect aircraft wing surfaces and rotor craft blades. These systems may not be suitable to protect engine inlets since any ice shed from leading nacelle surfaces can cause serious damage to engine components due to the high force of impact of ice particles. Furthermore, ice accretion on inlet nacelles distorts the intake airflow, thereby reducing the engine propulsion efficiency. Therefore, anti-icing systems are generally used to continuously maintain inlet surfaces free from ice.

This study is concerned with anti-icing systems, and in particular the thermal type (hot air and electro-thermal

* NRC Research Associate at *NASA Lewis Research Center*, Member AIAA
† Aerospace Engineer, Member AIAA

heaters). But the model developed may also be incorporated in the analysis of water, from thermally de-iced surfaces, that runs back downstream onto unprotected surfaces.

Recently, a runback model was developed [1,2,3] to better simulate the physics of water flow on aircraft surfaces. This was accomplished by incorporating a rivulet model for the streams of water often observed on airfoil surfaces during "running wet" anti-icing test cases. A computer code was developed to simulate running wet and evaporative aircraft anti-icing systems. This model is based on the analysis of the thin liquid water layer which forms in regions of direct impingement and, then, breaks up into rivulets in the vicinity of the impingement limits. The wetness factor distribution, F, resulting from the film breakup, and the rivulet configuration on the surface are predicted using a stability analysis theory and the laws of mass and energy conservation. The rivulets formed were assumed to be equally spaced as illustrated in Fig. 1. The value of F is updated from that location onward up to the point where total evaporation occurs, where the value of F becomes zero.

Several observations were made during experimental tests conducted in November 1991, in the NASA Lewis Icing Research Tunnel (IRT). Most of the data acquired were qualitative, some of which were reported in Reference [3]. Two of these observations are shown in Figs. 2 and 3. Figure 2 illustrates several rivulets running back to downstream regions on the surface of a thin leading edge body during one of the test cases. Upstream of the location where rivulet formation started, the entire surface was totally wet. Similarly, Fig. 3 shows a more definitive breakup of the thin liquid film into rivulets on an engine inlet cowl. Rivulets in the latter case were more consistently established due to the larger leading edge radius of the cowl. This triggers the significance of scaling when testing a sub scale model in a refrigerated spray tunnel. The qualitative experimental data agreed well with the code predictions.

In the current work, a series of experimental tests were conducted in the NASA Lewis IRT on an electro-thermally heated NACA 0012 airfoil. This study mainly includes quantitative comparisons between the experimental and the numerical surface temperature predictions to assess the validity of the current computer anti-icing model. An infrared camera was utilized to measure the instantaneous temperature profile of the outer skin. A general overview of the analytical model development will first be given. Then, discussions on the experimental setup as well as the numerical and test results will follow.

II. Analytical Model

II.1 Runback Water

The rate of water striking leading aircraft surfaces is relatively small. Consequently, its behavior is predominantly controlled by aerodynamic effects, water surface tension, and the physical properties of the aircraft skin. The surface tension phenomenon derives from intermolecular cohesive forces. The molecules in the thin layer of water of the impingement region are mainly subjected to attractive forces between neighboring molecules. At the water-air interfacial surface, an unbalanced cohesive force exists and is directed toward the liquid side. This unbalance causes the interfacial water molecules to move inwards. Consequently, the interface tends to contract which may lead to the breakup of the water film into beads (macroscopic drops) or rivulets (shallow and narrow streams). These phenomena are referred to as capillary phenomena. This explains many of the observations made earlier by Olsen and Walker [4], and later repeated by Reehorst et. al [5,6], in the NASA Lewis Icing Research Tunnel.

In the neighborhood of the stagnation line, relatively small water drops form due to the coalescence of many microscopic cloud droplets impacting the surface because of surface tension effects, as explained above. This is only true if the water is not evaporated by a thermal anti-icing system. When the drops grow large enough such that aerodynamic forces overcome the adhesion forces between the drops and the solid surface, they are swept back downstream on the aircraft skin. However, the surface in the direct impingement region is still considered entirely wetted. This is due to the incoming droplets that continuously tend to wet the surface between the water beads with a very thin liquid layer. This phenomenon was observed in the IRT during the previous [3] test as well as during the current tests. However, at the limits of impingement, the liquid film is most probably unstable due to surface tension forces, and it can no longer wet the entire surface. This causes the surface water to coalesce into individual streams, referred to as rivulets, separated by dry spaces.

In the analytical model, the rivulets formed are assumed to be equally spaced, with the cross-section of each rivulet having the shape of a portion of a cylinder. The angle between the surface and the line tangent to the curve representing the liquid-air interface at the triple point, is called the contact angle θ (see Fig. 1). It is a function of the liquid and the surface properties. The water flow on the surface is driven by the aerodynamic friction on the aircraft skin, and the flow is assumed to be along surface streamlines. Details on the hydrodynamics and stability analysis of shear driven thin liquid films may be found in Ref. [1], and its application to anti-icing systems modeling in Ref. [2].

The runback model utilized herein is based on a two-dimensional mathematical formulation. The surface water and the solid structure temperatures vary across their thicknesses and in the flow direction along a streamline on the surface. Spanwise temperature variation is assumed to be small. However, the latter is accounted for by performing energy balances on control volumes whose spanwise widths extend between two adjacent streamlines on the aircraft surface. The latter are determined from the flowfield solution.

Additional Feature:

The computer model was originally developed for anti-icing applications such that the heat required to keep the runback water from freezing is supplied to the surface, at the minimum. This is because a two-dimensional phase-change model was found to be inappropriate since freezing will normally start at the liquid-air interface, which creates a problem in modeling the flow characteristics of the unfrozen water. However, since the temperature drop across the film thickness is small, the temperature may be assumed to be uniform across the layer. Therefore, when a freezing temperature, or lower, is attained during the calculation process, an alternate method is used.

The method used consists of performing a macroscopic energy balance on the surface water to obtain the freezing fraction. This is defined as the ratio of water that freezes in a control volume to the total mass of liquid water entering the control volume. Nevertheless, the rivulet configuration and the method used for prediction of the wetness factor remains unchanged. This enables one to predict the amount and location of ice accumulation during a specified period of exposure time.

II.2 Anti-icing systems:

The current computer model was designed to handle two different types of thermal anti-icing systems: the hot air type, and the electro-thermal type. In the hot air type systems, hot air is generally drawn from an intermediate or high stage compressor bleed port or provided by a heating system through a heat exchanger. The air is then ducted through passages to the leading edges of wings, empennages, engine nacelles or other critical areas. Since the anti-ice air temperature distribution depends on the solid wall temperature distribution which also depends on the runback water solutions, the energy equations of those three regions must be solved simultaneously.

In the electro-thermal type systems, the heating elements are modeled as individual layers in the aircraft composite body structure. The mathematical formulation also allows anti-icing to be achieved by means of simply applying a specified heat flux distribution at the wall inner surface. This is provided as a user input option to the code. In addition, any combination of the three methods of heating is permitted. This type of formulation was chosen to give the flexibility of modeling different systems and to provide a tool that can be used in the design and analysis stages of the system development.

II.3 Wall Structure

Several different approaches are available to numerically simulate the temperature variations within the aircraft skin structure. The method used herein is the control volume approach. An equation is written for each node in the discretized region using the laws of energy conservation. This is an accurate method due to its conservation properties, specially when dealing with heat transfer across the interface of different property layers, and at the domain boundaries. The method also possesses a high numerical stability.

The temperature is assumed to vary in the streamwise direction and across the thickness of the wall. It is further assumed to be constant in the spanwise direction. However, the variation of the width of each strip in the spanwise direction (i.e., the distance between two adjacent surface streamlines) is accounted for in the energy balance equation of each control volume. For example, this width is constant for a two-dimensional flow over a 2D airfoil, and is variable for flow about an engine inlet nacelle or a tapered wing.

III. Computational Scheme

A simultaneous numerical solution of the governing energy and mass conservation equations must be obtained in the following three regions: (1) runback water; (2) solid structure; and, (3) anti-ice bleed air, if it is used. This is carried out using an iterative type of solution due to the dependency of the boundary conditions of each region on the final solution of its adjacent region.

A fully implicit method was used to numerically solve the runback water energy equation because of its positive stability properties. Backwards differencing in the streamwise direction, and central differencing in the transverse direction were employed. This produces a temperature distribution within the water layer thickness at each streamwise location. This distribution is then averaged locally to produce a single value of the local runback water temperature.

The governing energy equation of the anti-ice bleed air, is a first order ordinary differential equation (ODE). A very accurate and frequently used technique for solving ODE's, is the fourth order Runge-Kutta method. Knowing the temperature distribution in the wall, from the most recent iteration, the latter method is used to predict or update the hot air temperature distribution in the cowl. The result is subsequently used in the wall temperature solution at the next iteration.

Finally, the control volume approach was chosen to represent the heat balance on the wall structure as mentioned earlier. Difference equations are derived by performing an energy balance on each control volume corresponding to a particular node. Details of the numerical techniques and the iterative solution procedure between the regions of interest are presented in Ref [2].

IV. Experimental Setup

IV.1 Test Model

The current tests were conducted in the NASA Lewis Research Center Icing Research Tunnel (IRT) during the last two weeks of August, 1992. The test section in the IRT is 9 ft wide, and 6 ft high. The test model used is a NACA 0012 airfoil with 21 inch (0.533 m) chord, and 6 feet (1.829 m) span. It is centered vertically on the

turntable of the IRT Test Section to control the airfoil angle of attack with the air flow. It comprises a removable leading edge that measures 35 inches spanwise which fits on the center of the model. The 18.5 inch on each side of the center piece are non-active, while the center section is built to accommodate the ice protection system to be tested.

The center section has an active region where the surface is ice protected along a 32 inch strip along the span. It is a 0.25 inch thick fiberglass material which is covered with a thin layer of epoxy/glass insulation. The heater mats are then laid on top of the insulation material. The latter were divided into five isolated zones as illustrated in Fig. 4. The heating rate in each zone is individually controlled by a voltage Variac. The zone setup is as follows: Zone A is 0.5 inch (1.27 cm) wide centered at the leading edge, Zone B is on the upper side and zone C is on the lower side of A, 1.0 inch (2.54 cm) wide each; and, finally, Zones D&E, adjacent to B&C, respectively, at 1.5 inches (3.81 cm) wide each.

The heater mats were insulated on each side with a temperature/electrical resistance tape. An aluminum abrasion shield was laid on top of the heater mats. In between the two layers, a heat transfer grease was used to make a good thermal contact between the heaters and the aluminum shield to increase the heat transfer performance and reduce the possibility of delamination of the layers.

The current test served two purposes. *Technology Dynamics Group, Inc.*, the developers of the new technology heater mats, were interested in testing the operation and performance of their product as an anti/de-icer system, while one of NASA Lewis's interests was to expand their existing experimental database to support in-house computer code validation.

IV.2 Infrared Temperature Measurements

There exist several commercial types of non-contact temperature measurement instruments. Most of them rely on the same basic principles. All objects emit radiant energy which increases with increasing surface temperature of the object.

The emitted energy is distributed over a band of wavelengths in the electromagnetic spectrum. This distribution may be represented by a curve known as the Planck function. The peak of this curve shifts towards the shorter wavelength regions as the object surface temperature increases.

Objects which are at near room temperature have spectral energy distributions that peak near the middle of the infrared region (i.e., close to 10 microns). The radiated energy is received by a radiant sensitive instrument which is calibrated to translate the energy intercepted into temperatures using the appropriate relationship between the two variables.

Eventually, a portion of the radiated energy is absorbed by the atmospheric medium that exists between the object and the temperature reading instrument. Typically, the majority of the absorbed energy is due to the water vapor in the atmosphere. However, energy absorption is almost negligible in the long wave range (8-14 μm) of the electromagnetic spectral band.

The instrument used herein for surface temperature measurements is the Inframetrics Model 600 IR system which is designed to intercept radiant energy in the band of 8 to 14 μm. Generally, most non-metallic materials have high emittance in this region. However, the majority of metallic surfaces have a low emittance. For example, Aluminum has an emittance value of as low as 0.04, depending on its purity and surface polish. In the current experimental setup, the airfoil model had an Aluminum abrasion shield with high reflectance. In order to increase its emissivity and to eliminate any reflectance from other objects, the surface was coated with a thin layer of flat black paint. Consequently, the emissivity of the surface is increased to about 0.95.

The infrared scanner and analyzer setup used in the test is the Inframetrics Model 600. This model has a very high frame rate which allows data to be viewed without any sacrifice of time delay or accuracy. The system provides a video output signal that is fully compatible with the NTSC television standard.

The IR camera was set in the IRT control room to monitor the surface of the airfoil (almost perpendicularly). The center window of the tunnel observation room was replaced with a Plexiglass window with a hole drilled in it to allow viewing the model with the IR scanner. A 4.75 inch diameter CLEARTRAN™ clear window (water clear zinc sulfide) access port was inserted in that hole. It possesses attractive optical properties since it can transmit radiant energy in the visible through the infrared range (0.4-16 microns) of the spectrum. Its transmittance for that range is approximately 0.7.

A few problems were encountered with using the CLEARTRAN™ window. The cold temperature inside the tunnel test section caused a tremendous amount of water condensation on the window of the control room side. To overcome this problem, a heat gun was used to keep the surface clean. However, the amount of heat required to achieve that objective caused an increase in the window temperature which affected the IR camera surface temperature readings. This may be associated with the high reflectance of the window surface as well as its heat absorption.

Finally, the best solution to these problems was to use a small sliding window that may be opened during the data acquisition and closed afterwards to reduce the noise level in the control room. Thus, no obstructions exist between the scanner and the airfoil surface. Consequently, no calibration was required for the scanned temperature readings except for the surface emissivity and radiant energy absorbed by the water droplet cloud.

IV. Experimental Results and Comparison to Numerical Calculations

Although the tests consisted of de-icing as well as anti-icing runs, only the latter are of concern in the present discussion. In these cases, the airfoil was mounted vertically on the turntable in the IRT such that the angle of attack of the airfoil with the flow was 4 degrees. The lower surface (pressure side) was visually and instrumentally monitored from the control room through heated windows and access ports.

The complete numerical solution to the problem was resolved in three major steps: (1) flowfield calculations, including the viscous layer near the wall; (2) individual water droplet trajectory calculations using the velocities calculated in the previous step; and, finally, (3) the heat transfer calculations to determine the surface water and skin temperature distributions.

The flowfield around the airfoil must be calculated such that viscous effects near the wall are accounted for. This can be accomplished with a non-viscous flow solver which includes a boundary layer model. On the other hand, it may be accomplished using a code that numerically solves the full or a simplified version of the Navier-Stokes equations. ARC2D, a "thin layer" Navier-Stokes solver developed at NASA Ames, was used for this purpose. It has been used lately for icing-studies at NASA Lewis by Potapczuk [7], and was found to give satisfactory results for low angles of attack. The model is adequate for high Reynolds number, and for attached and mildly separated flows where the viscous terms associated with derivatives in the direction parallel to the body are negligible. The output format from the code was tailored to the inputs requirements of the current heat transfer code.

The resulting pressure coefficient and friction coefficient distributions from ARC2D are illustrated in Figs. (5) and (6), respectively. These coefficients are defined as follows:

$$C_p = \frac{P - P_\infty}{\frac{1}{2}\rho_\infty V_\infty^2} \qquad (1)$$

and,

$$C_f = \frac{\tau}{\frac{1}{2}\rho_\infty V_\infty^2} \qquad (2)$$

The first coefficient may be used to calculate properties at the edge of the boundary layer, and the second is used to compute the wall shear stress that causes the water to run back.

Due to the effects of viscosity near the solid surfaces, large gradients of the variables exist in these regions. This requires a fine grid spacing in the directions normal to the rigid body which allows the flow solver to capture all the necessary details in those regions. To accomplished this, a hyperbolic grid generator was used to produce a C-type grid structure around the airfoil. The resulting curvilinear body fitted mesh was composed of: (309 grid points along the surface) by (65 nodes in the nearly normal direction).

The droplet trajectory and impingement module of NASA's ice accretion code LEWICE [8], originally developed by *FWG Associates* under a contract for NASA Lewis, was used to generate the collection efficiency curves. The code was modified by Potapczuk [7] to read and interpolate the flowfield velocities from the outputs generated by ARC2D. Minor modifications were also required for the code to handle viscous flows when the flowfield code is run in a viscous mode (Navier-Stokes equations) as opposed to non-viscous compressible mode (Euler equations).

The particle trajectories were subsequently used to compute the local collection efficiencies. The cloud was assumed to be mono-dispersed with a droplet size of either MVD = 15 μm, or MVD = 20 μm, depending on the particular case being considered. The corresponding results are respectively shown in Figs. 7 and 8 for the different air speeds used during the tests.

In an earlier discussion, it was mentioned that when runback water exists on the surface it will flow back as rivulets, or a combination of water beads and rivulets, beyond the impingement region. Previous observations [3] showed that pure rivulet flow structure is more probable to exist on blunt bodies than on thin leading edge bodies as illustrated in Figures 2 and 3. As expected, since the airfoil used in the current test may be considered as a thin leading edge body, the current observations agreed with the above conclusion.

Individual beads were seen to flow on the surface in cases of low mass flow rates. These cases correspond to at least one of the following conditions: (1) low liquid water contents, (2) low freestream velocities, and, finally, (3) high rates of evaporation caused by high power densities applied to the surface in the impingement regions. Another reason for the formation of water beads is the highly smooth solid surface which decreases the adhesion forces between the drops and the surface, consequently increasing the contact angle θ (see Fig. 1). Once rivulets were seen to leave the direct impingement region, they froze in downstream regions for two reasons: (1) the downstream regions were thermally unprotected, (2) less heat was absorbed by the rivulet due to the decreased wetting factor.

Moreover, when large beads formed on the smooth and thin leading edge body surface, they moved slowly in the downstream direction near the stagnation line. However, once the beads moved slightly beyond the stagnation region, they ran back at a much faster speed onto unprotected regions. This is due to the rapid increase in the local aerodynamic shearing forces as was illustrated in Fig. 6. The drawback in this situation is that the amount of heat absorbed by those beads diminishes drastically due to the decrease in residency time of the drops in the heated region, normally the region of direct impingement and slightly further downstream. Consequently, total evaporation should be

carefully accomplished as early as possible without inducing any probable damage to the heater mats or the structure.

Several operating conditions were considered in the current tests. In the earlier runs, the model failed after several hours of operation. One of the main reasons associated with this failure, burnout at different spots, was that the substrate was only able to handle a maximum temperature of about 250°F. In addition, the heater mats were initially laid on the substrate surface without a heat insulating material. This problem was resolved by using a layer or two of glass epoxy as an insulating material.

Another problem encountered was the relatively long period required for the system to reach a steady state when running in an anti-icing mode. This problem was not expected to occur, and, therefore, many data points were collected at an earlier time than required for the system to stabilize. This problem was not detected until later during the test from thermocouple temperature readings. The cause for this long period that was required for a stable condition to be reached was mainly associated with a heat transfer grease that was applied between the heater mats and the abrasion shield, as mentioned earlier.

The idea behind the use of the grease was to make a better physical contact between the heater mats and the abrasion shield, and to eliminate the possibility of the existence of air gaps. This, supposedly would increase the system performance. However, although the grease had a very good thermal conductivity property, its thermal capacitance (product of density and specific heat) was very high. Consequently, the grease took a long time to warm up when the heaters were fired on. Later, when the power density is reduced or the heaters shut off, the grease also took a longer period to cool down due to the large amount of heat initially absorbed. Subsequently, at least five minutes were allowed for the system to stabilize before recording the actual data.

One of the difficulties with measuring the surface temperature using an IR camera is calibration. The IR scanner has different settings, user defined, for the range of temperature to be measured. A separate control is then provided to set the center temperature within the predefined range. The smallest range that may be used is 5°C. However, this is not sufficient enough for such measurements since the surface temperature may vary from about freestream temperature to the neighborhood of 25°C. This temperature range can be greater than 50°C. The problem with such a high range settings on the IR scanner is that the error in temperature readings increases with increasing temperature range settings. This had to be taken into account with some degree of difficulty with the calibration. Mainly, the temperatures were calibrated against regions downstream of the heated zone, where the surface temperature would be known to be in the neighborhood of the freestream temperature. Figure 9 illustrates a sample video output from the IR scanner (the original scan is in color).

Nevertheless, the cases that were considered in this report were chosen such that most of the problems mentioned earlier either did not exist or had been eliminated. Those cases are summarized in Table 1. They represent five different operating conditions: freestream temperature, velocity, liquid water content, mean volume droplet diameter, and power densities. The airfoil was set at 4 degrees angle of attack in all cases. Since only the lower surface was monitored by the infrared camera for surface temperature measurements, the results shown in the following sections correspond to that side only of the airfoil surface. In the following figures, "s" represents the distance from stagnation on the surface and is negative on the lower surface (pressure side).

The summary of results are shown in the last column of Table 1. In Cases 1 and 2, the table clearly shows that the system, when running in an anti-icing mode, was able to completely evaporate the water impinging on the surface before it ran back to the unprotected downstream regions. However, in cases 3 through 5, the heat supplied to the surface was only able to partially evaporate the surface water, which eventually ran back and froze at some distance downstream.

Figures 10 and 11 represent the surface temperature distribution, and, the runback mass flow rate and freezing fraction distributions for Case 1, respectively. The corresponding variables are plotted in Figs. 12 and 13 for Case 2, respectively. These results show that the experimental surface temperature readings are in good agreement with the code predictions in Case 2. The differences shown in Fig. 10 for Case 1 are slightly above the experimental margin of errors. This may be associated with the poor code prediction of the heat transfer coefficient distribution between the surface and the freestream air. However, the agreement was perfect regarding the prediction of total evaporation. Figures 11 and 13 show that only a very small amount of liquid water (because $FF = 0$) exists in direct impingement region in these two cases. However, total evaporation of the water is achieved upstream of the impingement limits.

In Cases 3 and 4, as shown in Figs. 14 through 17, the runback water froze downstream of the heated regions. The location where freezing begins corresponds to the location where the freezing fraction FF goes above the value of zero. This corresponds to the computer predicted surface distance of approximately 0.095 m from the stagnation point for Case 3, as shown in Fig. 15. The close-up video from the experimental observations showed that freezing for that case occurred at a distance of about 0.11 m. In Case 4, the freezing location was predicted at about 0.11 m, and the corresponding experimental observations showed that this occurred at about 0.1 m. This distance varied spanwise during the experiment by at least 0.01 m in all the cases. Therefore, the computer predictions are considered to be in very good agreement with the test results.

The surface temperature predictions for the latter two cases are shown in Figs. 14 and 16. The agreement is very good in Case 3 and is relatively good in Case 4. Note that in Case 4, the numerical code predicts a plateau region where the surface temperature is zero degrees Celsius. This is due to the assumption that the water/ice mixture (freezing fraction is larger than zero and smaller than one) remains at zero degrees Celsius until all the water freezes. However, this is not what was actually predicted by the IR camera. It seems that the temperature continuously decreases in some fashion.

The same is true for the surface temperature predictions of Case 5, as shown in Fig. 18. A couple of reasons may be associated with the disagreement of results. One reason may be due to the fact that the accumulated ice is cooling below freezing, while the water that remains unfrozen runs back in the valleys between frozen rivulets. The other reason, which is less likely to tremendously affect the measurements, is that the IR scanner is calibrated for surface temperatures of above – 20 °C. Notice that the cases where marginal agreement occurred between the numerical and experimental results are those which correspond to a very cold freestream condition ($T_\infty = -17.78$ °C). These correspond to Cases 1, 4, and 5. This also causes the outer layer of the frozen ice to cool faster than the liquid water running between the valleys.

Inspection of the operating conditions given in Table 1 shows that the only difference between Case 4 and Case 5, is that the freestream velocity in the latter case is twice that of Case 4. This generally means that the rate of water catch on the surface is almost doubled, which explains why more runback froze downstream. The freezing also occurred earlier (shorter distance from stagnation) within the heated region. The reason for this is the increase in the heat transfer coefficient to the ambient. Thus, the heater in zone E was turned off since it would not help with the power density settings of 20 W/in^2 which were used in Zone A and Zone C. In this case, higher power densities would be required. However, in Case 4, the runback froze beyond the heated zones. In both cases, it is recommended that the heated zone be extended a little further downstream. This is specially true for high LWC and freestream velocity, since increasing the power density alone to that required to achieve total evaporation would be extremely high such that the heater mats and/or the structure could be damaged from the elevated surface temperature.

Finally, it should also be noted that the first two cases, where total evaporation was achieved, represent cloud conditions of relatively low liquid water content (LWC = 0.5 g/m^3) compared to the other cases (LWC = 1.0 g/m^3). The lower temperature conditions contributed less than the high LWC to runback beyond the heaters. This may be seen by comparing results of Case 1 and Case 4 where the freestream temperature was – 17.78 °C and the major difference between the two cases was the high LWC in Case 4 where the runback froze.

V. Concluding Remarks

The analysis developed earlier confirmed that the liquid water film which forms in regions of direct droplet impingement will breakup into beads and/or rivulets in the neighborhood the impingement limits. Despite some experimental difficulties, very good agreement was generally obtained between the numerical predictions of the computer code and the experimental results of surface temperature. For cases where the freestream temperature was extremely cold, the agreement was acceptable. The location where the runback water may freeze, if conditions favor it, was well predicted by the computer model.

An efficient anti-icing system design may be achieved with a sufficient heat supply to the regions of direct impingement within the tolerable limits of the aircraft structural materials for two reasons. The first is due to the fact that runback water flows fast past the heated regions such that its residency time in those regions is not sufficient to achieve total evaporation. The other reason is that more heat is transferred to the water to evaporate it in the impingement region and less heat is lost to the ambient compared to the heat loss through dry areas on the surface in the downstream regions. Under extreme weather conditions, the heated zones should also be extended further downstream to achieve complete evaporation of the runback water and prevent it from freezing.

Future work should include a larger set of experimental data now that many of the issues regarding the IR scanner and packaging of the anti-icing system have been addressed and mostly resolved. This is vital in the validation of computational simulation computer codes. Furthermore, the details of the water and ice behavior at the freezing point should be carefully looked at to determine the temperature behavior of the ice/water mixture, and the distance over which the frozen rivulets extend and to what thickness for a given exposure time.

Acknowledgments

This work was done while the first author held a *National Research Council* Research Associateship at *NASA Lewis Research Center*. The sponsorship of these two organizations is gratefully acknowledged. Also, the cooperation of George Grauer from *Technology Dynamics Group, Inc.*, and Tomas Bond from *NASA Lewis* with the experimental tests is well appreciated.

References

1. Al-Khalil, K.M., Keith, T.G., and De Witt, K.J., "Development of an Anti-Icing Runback Model," AIAA Paper 90-0759, Jan. 1990.

2. Al-Khalil, K.M., Keith, T.G., and De Witt, K.J., "Further Development of an Anti-Icing Runback Model," AIAA Paper 91-0266, Jan. 1991.

3. Al-Khalil, K.M., Keith, T.G., and De Witt, K.J., "Development of an Improved Model for Runback Water on Aircraft Surfaces," AIAA Paper 92-0042, January 1992.

4. Olsen, W., and Walker, E., "Experimental Evidence for Modifying the Current Physical Model for Ice Accretion on Aircraft Surfaces," NASA TM-87184, May 1986.

5. Hansman, R.J., Reehorst, A., and J. Sims, "Analysis of Surface Roughness Generation in Aircraft Ice Accretion," AIAA Paper 92-0298, Jan 1992.

6. Hansman, R.J., Breuer, K., Hazan, D., Reehorst, A., and Vargas, M., "Analysis of Surface Roughness Generation in Aircraft Ice Accretion," AIAA Paper 93-0029, Jan 1993.

7. Potapczuk, Mark G., "LEWICE/E: An Euler Based Ice Accretion Code," AIAA Paper 92-0037, Jan 1992.

8. Ruff, G.A., and Berkowitz, B.M., "Users Manual for the NASA Lewis Ice Accretion Prediction Code (LEWICE)," NASA CR-185129, May 1990.

Table 1: Operating Conditions for the different Cases.

Case #	T_∞ (°C)	V_∞ (mph)	LWC (g/m^3)	MVD (μm)	Power density (W/in^2)			Comments on results
					Zone A	Zone C	Zone E	
1	– 17.78	100	0.50	15	15.0	15.0	7.5	a
2	– 6.11	100	0.50	15	15.0	15.0	5.0	a
3	– 6.11	100	1.00	20	15.0	15.0	5.0	b
4	– 17.78	100	1.00	20	20.0	20.0	10.0	b
5	– 17.78	200	1.00	20	20.0	20.0	0.0	b

a- Total evaporation of the impinging water was achieved.

b- Partial evaporation and freezing runback.

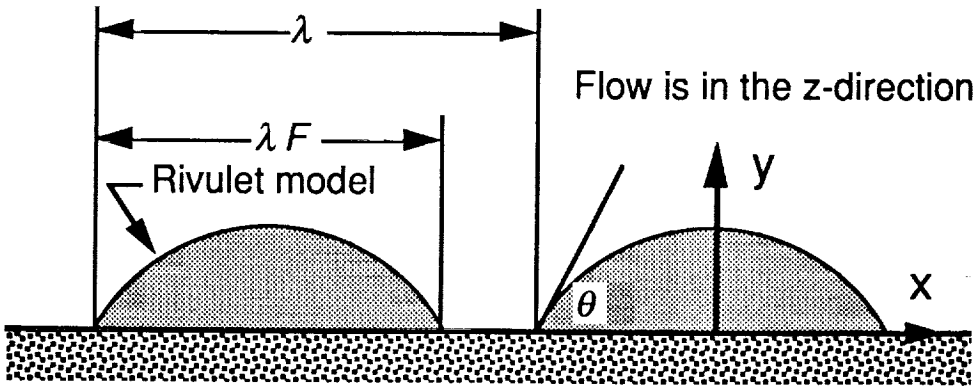

Fig. 1: Resulting rivulets after breakup of the film in the impingement region.

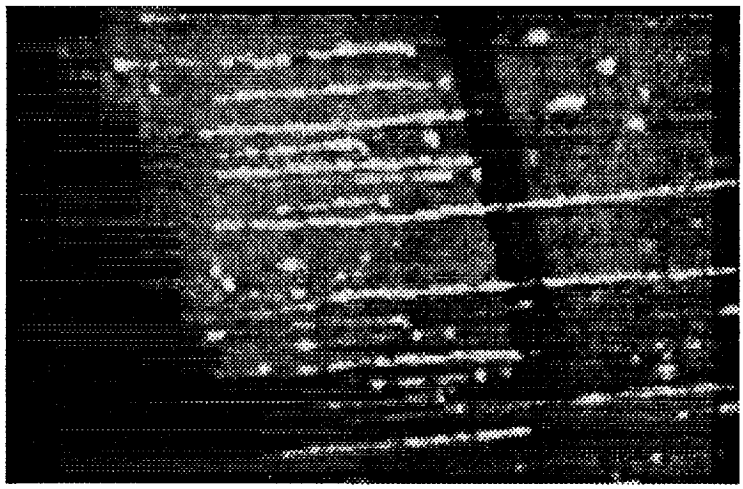

Fig. 2: Runback rivulets on a thin leading edge body in the IRT.

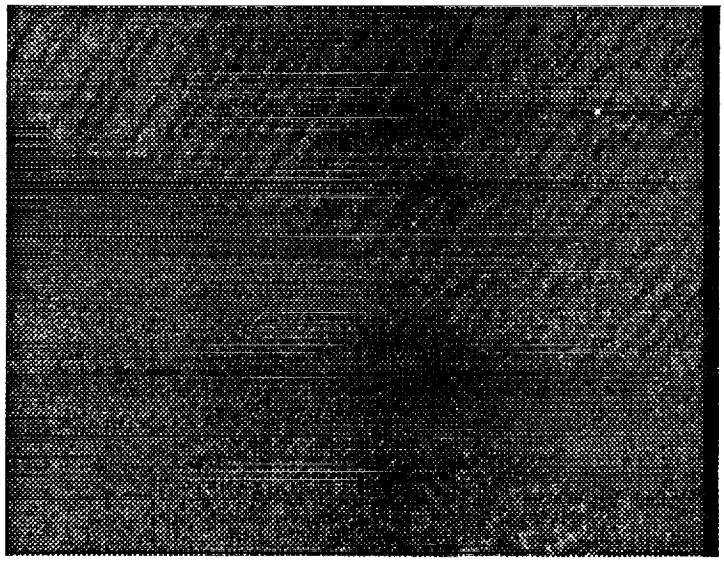

Fig. 3: Runback rivulets on an engine inlet cowl in the IRT.

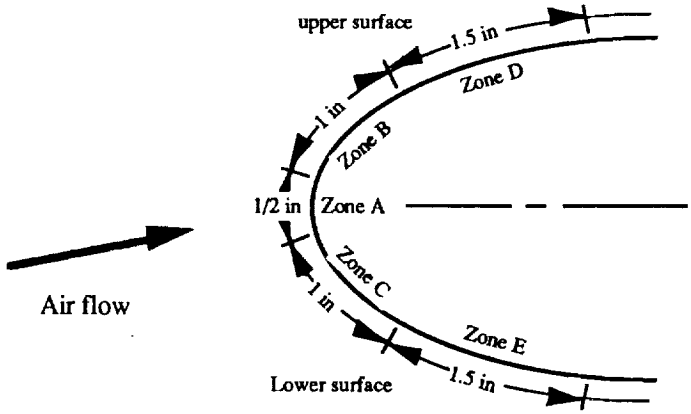

Fig. 4: Heater zones on the airfoil leading edge.

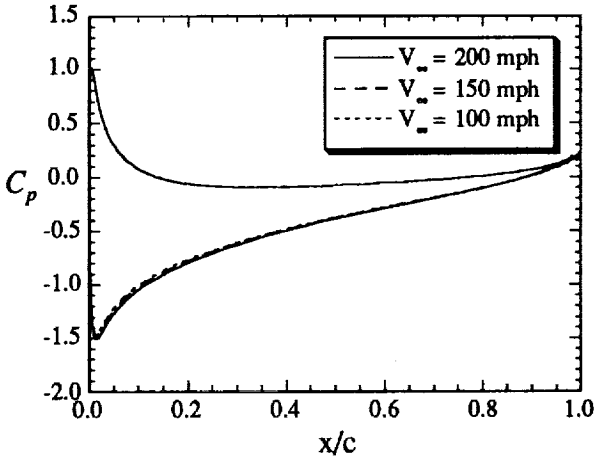

Fig. 5: Surface pressure coefficient.

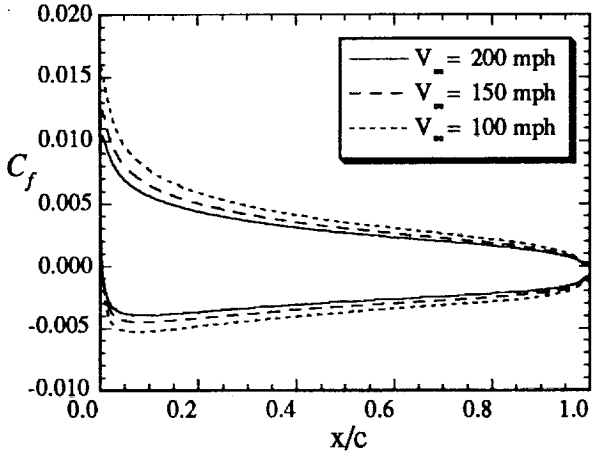

Fig. 6: Surface friction coefficient.

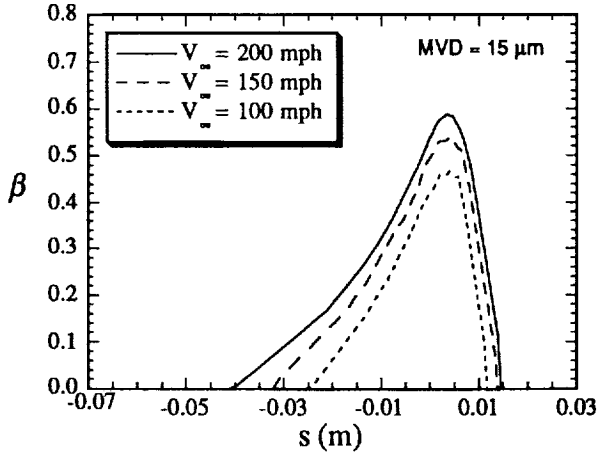

Fig. 7: Droplet collection efficiency (MVD = 15 μm)

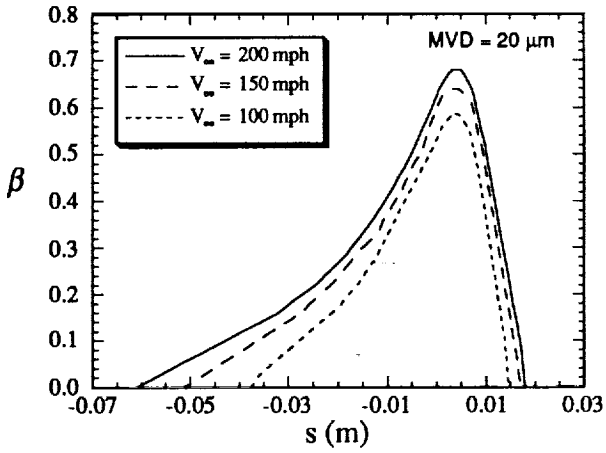

Fig. 8: Droplet collection efficiency (MVD = 20 μm)

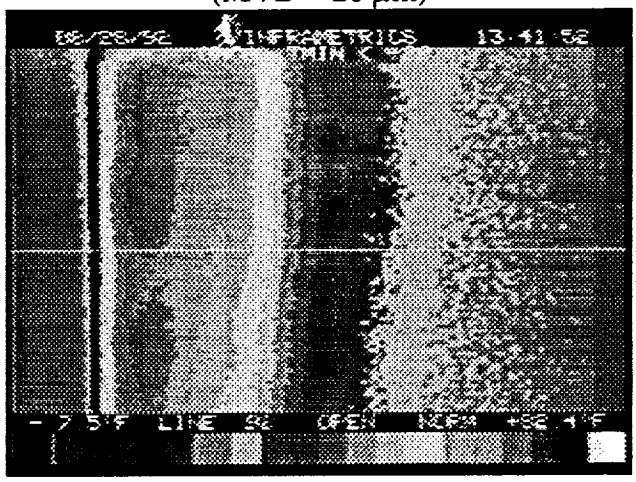

Fig. 9: An Example of IR Temperature Reading from the Airfoil Surface.

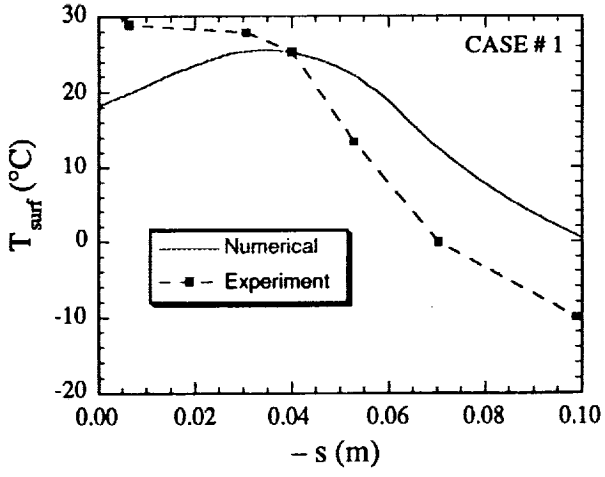

Fig. 10: Surface temperature for Case # 1.

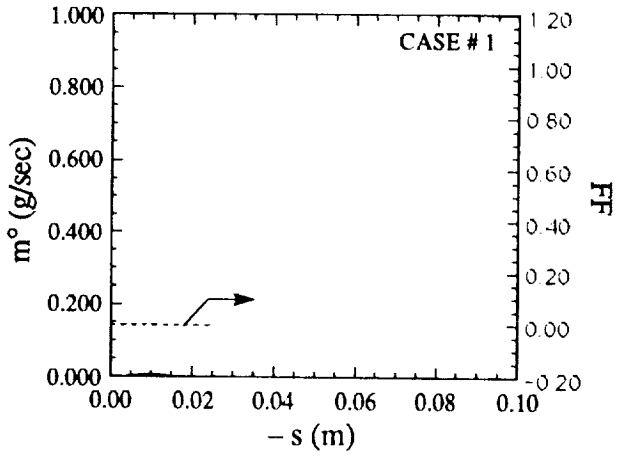

Fig. 11: Predicted runback mass flowrate & freezing fraction for Case # 1 (lower surface).

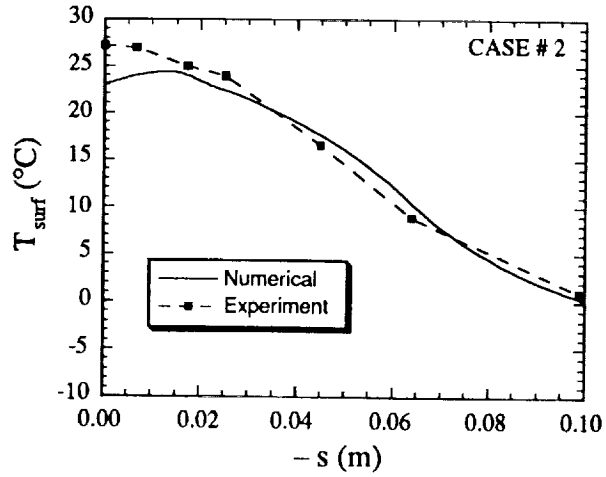

Fig. 12: Surface temperature for Case # 2.

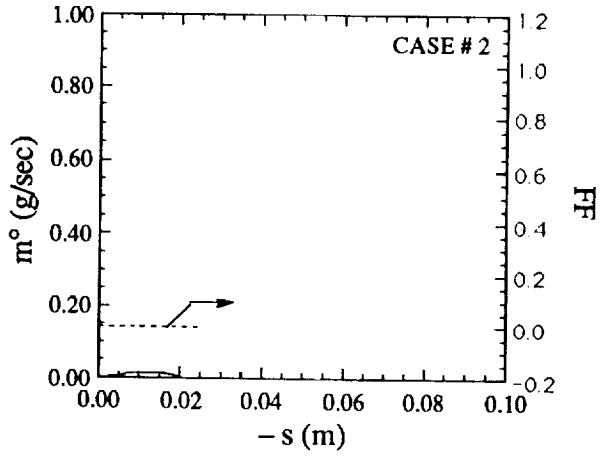

Fig. 13: Predicted runback mass flowrate & freezing fraction for Case # 2 (lower surface).

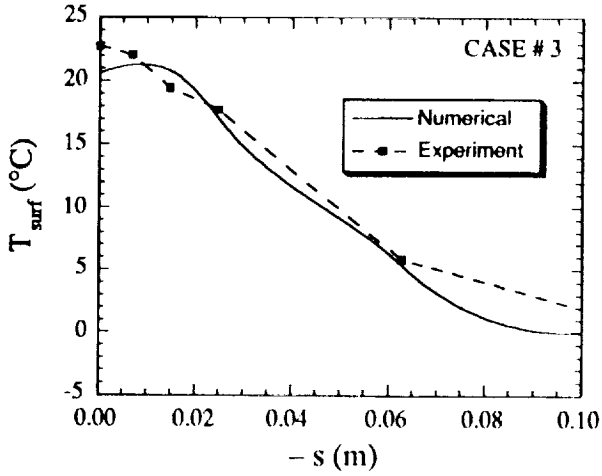

Fig. 14: Surface temperature for Case # 3.

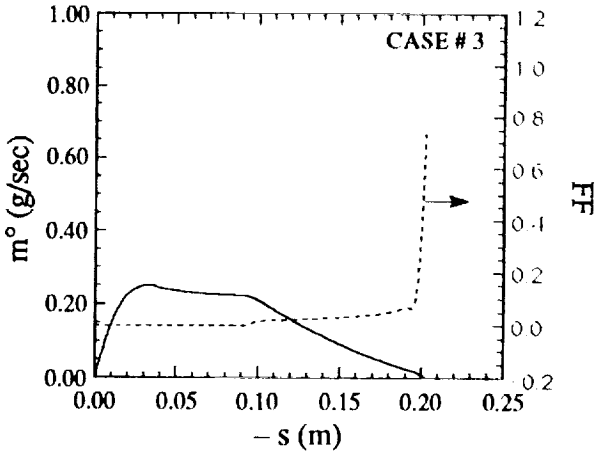

Fig. 15: Predicted runback mass flowrate & freezing fraction for Case # 3 (lower surface).

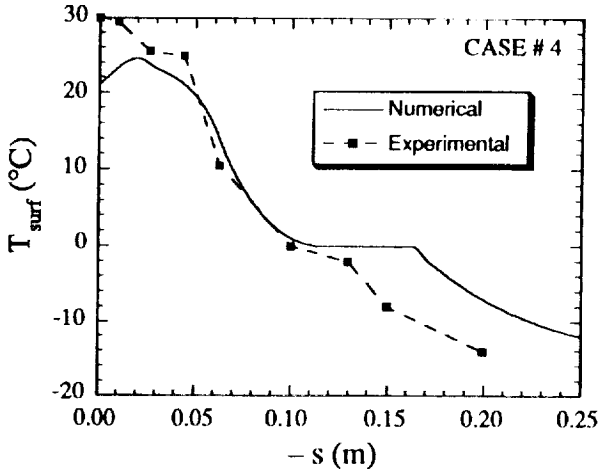

Fig. 16: Surface temperature for Case # 4.

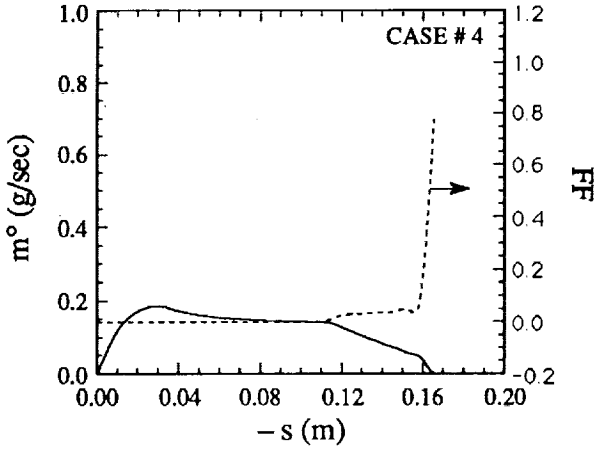

Fig. 17: Predicted runback mass flowrate & freezing fraction for Case # 4 (lower surface).

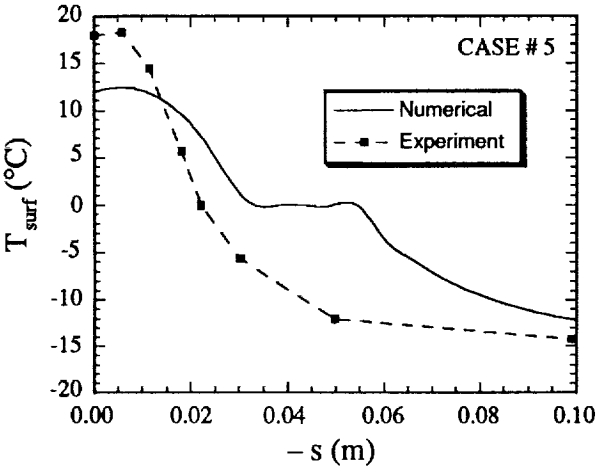

Fig. 18: Surface temperature for Case # 5.

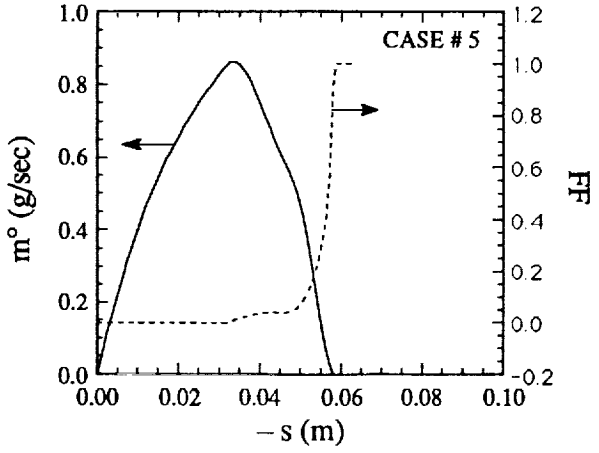

Fig. 19: Predicted runback mass flowrate & freezing fraction for Case # 5 (lower surface).

REPORT DOCUMENTATION PAGE

Form Approved
OMB No. 0704-0188

1. AGENCY USE ONLY (*Leave blank*)	2. REPORT DATE	3. REPORT TYPE AND DATES COVERED
	January 1993	Technical Memorandum

4. TITLE AND SUBTITLE

Numerical Modeling of Anti-Icing Systems and Comparison to Test Results on a NACA 0012 Airfoil

5. FUNDING NUMBERS

WU-505-68-10

6. AUTHOR(S)

Kamel M. Al-Khalil and Mark G. Potapczuk

7. PERFORMING ORGANIZATION NAME(S) AND ADDRESS(ES)

National Aeronautics and Space Administration
Lewis Research Center
Cleveland, Ohio 44135-3191

8. PERFORMING ORGANIZATION REPORT NUMBER

E-7498

9. SPONSORING/MONITORING AGENCY NAMES(S) AND ADDRESS(ES)

National Aeronautics and Space Administration
Washington, D.C. 20546-0001

10. SPONSORING/MONITORING AGENCY REPORT NUMBER

NASA TM-105975
AIAA-93-0170

11. SUPPLEMENTARY NOTES

Prepared for the 31st Aerospace Sciences Meeting and Exhibit sponsored by the American Institute of Aeronautics and Astronautics, Reno, Nevada, January 11-14, 1993. Kamel M. Al-Khalil, National Research Council-NASA Research Associate at Lewis Research Center. Mark G. Potapczuk, NASA Lewis Research Center. Responsible person, Kamel M. Al-Khalil, (216) 433-4601.

12a. DISTRIBUTION/AVAILABILITY STATEMENT

Unclassified - Unlimited
Subject Categories 02 and 03

12b. DISTRIBUTION CODE

13. ABSTRACT ***(Maximum 200 words)***

A series of experimental tests were conducted in the NASA Lewis IRT on an electro-thermally heated NACA 0012 airfoil. Quantitative comparisons between the experimental results and those predicted by a computer simulation code were made to assess the validity of a recently developed anti-icing model. An infrared camera was utilized to scan the instantaneous temperature contours of the skin surface. Despite some experimental difficulties, good agreement between the numerical predictions and the experiment results were generally obtained for the surface temperature and the possibility for the runback to freeze. Some recommendations were given for an efficient operation of a thermal anti-icing system.

14. SUBJECT TERMS

Anti-icing; Ice protection

15. NUMBER OF PAGES

14

16. PRICE CODE

A03

17. SECURITY CLASSIFICATION OF REPORT	18. SECURITY CLASSIFICATION OF THIS PAGE	19. SECURITY CLASSIFICATION OF ABSTRACT	20. LIMITATION OF ABSTRACT
Unclassified	Unclassified	Unclassified	